Elevation of Vernier thresholds during image motion depends on target configuration

Harold E. Bedell*

College of Optometry, University of Houston, Houston, Texas 77204-6052

Susana T. L. Chung

School of Optometry, Indiana University, Bloomington, Indiana 47405-3680

Saumil S. Patel

College of Optometry, University of Houston, Houston, Texas 77204-6052

Received July 21, 1999; revised manuscript received December 2, 1999; accepted February 7, 2000

Previously we showed that thresholds for abutting Vernier targets are unaffected by motion, as long as the targets are processed by the same spatial-frequency channel at each velocity and remain equally detectable [Invest. Ophthalmol. Visual Sci. (Suppl.) **37**, S734 (1996)]. In this study we compared Vernier thresholds for stationary and moving abutting and nonabutting targets (gaps = 0, 18, and 36 arc min) for velocities of 0–16 deg/s. The Vernier targets were spatially filtered vertical lines (peak spatial frequency = 3.3 or 6.6 c/deg), presented at contrast levels of two, four, and eight times the detection threshold of each component line. Unlike the results for abutting targets, Vernier thresholds for nonabutting targets worsen with velocity as well as gap size. The results for abutting Vernier targets are consistent with the hypothesis that thresholds are mediated by oriented spatial filters, whose responses increase proportionally with the stimulus contrast. The velocity-dependent thresholds found for nonabutting Vernier targets can be explained on the basis of local-sign comparisons if the comparison process is assumed to include a small amount of temporal noise. © 2000 Optical Society of America [S0740-3232(00)01806-8]

OCIS codes: 330.1070, 330.1800, 330.4150, 330.5510, 330.6100, 330.7310.

1. INTRODUCTION

Under a range of stimulus conditions, the threshold for discriminating spatial offset in a Vernier target is finer than the retinal photoreceptor mosaic, the defining characteristic of a hyperacuity.[1,2] Over the past several years, evidence has accumulated that the visual system achieves fine Vernier thresholds by using different mechanisms, depending on the characteristics of the stimulus. The most acute Vernier thresholds, obtained for highly visible, abutting line targets in the fovea, are thought to be mediated by the contrast responses of linear, oriented cortical filters that straddle the Vernier offset.[3–6] Thresholds are higher, but can remain within the hyperacuity range, when the Vernier targets are separated by more than a few min of arc[7–10] or have opposite contrast polarities.[11,12] The thresholds obtained under these stimulus conditions have been attributed to a local-sign mechanism that was first proposed by Hering.[13] According to this view, the locations, or position tags, of the individual Vernier elements are separately computed and then compared at a second stage.[8]

Vernier thresholds for high-contrast, abutting line stimuli are unaffected by linear motion up to a few deg/s but deteriorate at higher target velocities.[14–17] Previously we showed that the most effective stimulus for masking the Vernier offset of abutting line stimuli shifts to progressively lower spatial frequencies as the velocity of the stimuli increases.[17] This result implies that Vernier thresholds are elevated during motion primarily because larger spatial filters are used to discriminate the Vernier offset and not solely because of a reduction in stimulus visibility due to motion smear. Support for this interpretation comes from the subsequent finding that Vernier thresholds for stationary and moving abutting targets are identical as long as the targets are presented at an equal level of detectability and to the same spatial-frequency channel.[18]

Here we extend our previous results by comparing Vernier thresholds for stationary and moving targets that are nonabutting. The goal was to determine to what extent the putative local-sign mechanism, which should mediate Vernier thresholds for nonabutting targets, is robust to target motion. We presented Vernier targets at equal multiples of the contrast-detection threshold to prevent differences in detectability from influencing the Vernier thresholds. Further, targets were spatially filtered so that the mechanisms mediating detection of the targets are likely to be similar to those responsible for discriminating the Vernier offset. We found that unlike the results for abutting targets, Vernier thresholds for nonabutting, filtered stimuli worsen with image motion. Our data are consistent with an additive-variance model that may explain how the local signs of the two elements of a Vernier target are compared for moving targets.

0740-3232/2000/060947-08$15.00 © 2000 Optical Society of America

2. METHODS

Two-line, vertical Vernier targets were spatially filtered by use of a two-dimensional, circularly symmetric exponential filter with a peak spatial frequency of either 3.3 or 6.6 c/deg (Fig. 1). Bandwidth of the filter, expressed as the full width at half-height, was 1.5 octaves. Before filtering, each vertical line was 1.13 min wide by 18.15 min long. Filtering was carried out with the HIPS software[19] for line pairs with vertical gaps of 0 (i.e., abutting), 18, and 36 arc min and a range of horizontal offsets. The filtered targets were stored as digital images and were presented on a monochrome monitor (Image Systems, Hopkins, Minn.) at 240 Hz with use of a VSG2/3 board (Cambridge Research Systems, Cambridge, UK) housed in a 486 personal computer. The monochrome monitor was equipped with an ultrafast decay phosphor, DP104, which has a peak luminance output at ~565 nm and a spectral bandwidth of ~90 nm. The luminance of an intensified spot diminishes to <1% in ~250 μs. The mean luminance of the monitor was 50 cd/m^2. The monitor screen was surrounded by a 6.4 × 5.4 deg cardboard mask, illuminated to approximately the same color and luminance through combinations of polycarbonate filters (Edmund Scientific, Barrington, N.J.). Image motion was produced by viewing the target and surround from a front-surface mirror, mounted on a galvanometer (General Scanning G300, Watertown, Mass.) that was driven by a ramp wave form. The ramp wave form was generated by a programmable function generator (Hewlett Packard 3318A) that was, in turn, controlled by the personal computer via an IEEE interface card (B&C Microsystems, Sunnyvale, Calif.). On each trial, the observer first viewed a stationary black fixation square of approximately 0.2 × 0.2 deg followed, after a 250-ms blank interval, by a 150-ms presentation of the Vernier target. This stimulus duration, as well as the random presentation of leftward and rightward target motion, were chosen to minimize pursuit eye movements. Observers viewed the stimulus display monocularly with the right eye from an optical distance of 8 m. At this distance, one screen pixel corresponded to 17 arc sec.

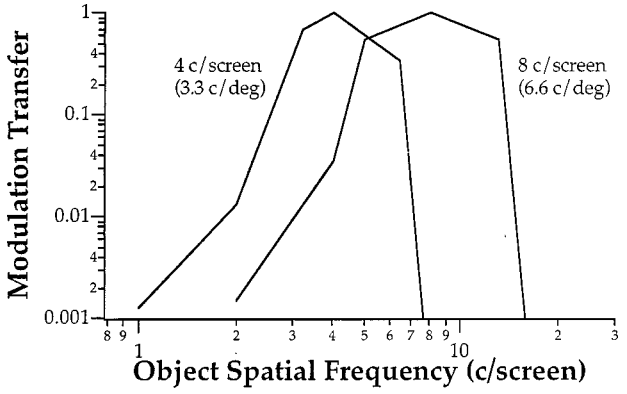

Fig. 1. Modulation transfer functions of the bandpass filters used in this study. The output amplitude of a sine-wave grating after filtering is normalized to the input amplitude and plotted as a function of object spatial frequency (c/screen). The object center frequency of these filters are 4 and 8 c/screen. At a viewing distance of 8 m, the center frequencies of these filters correspond to 3.3 and 6.6 c/deg, respectively.

To ensure that all Vernier targets were equally detectable, we first measured each observer's contrast-detection thresholds for a single filtered line centered at fixation for the 0-gap (abutting) condition and at 18 and 27 arc min above and below the center of the fixation target for the 18- and 36-min gap conditions, respectively. Previously, Klein *et al.*[20] showed that the detection thresholds for one line and for both lines of an abutting Vernier target are identical. Contrast thresholds were determined separately for each combination of target spatial frequency and velocity. The 3.3-c/deg targets were tested at four velocities: 0 (stationary), 4, 8, and 16 deg/s. The 6.6-c/deg targets were tested at 0 and 4 deg/s only, because their elevated detection thresholds prevented us from presenting these targets at sufficiently high multiples of the contrast threshold at faster velocities. Data for targets of 3.3 and 6.6 c/deg were collected at different times, about 2 months apart. A two-alternative, temporal-forced-choice paradigm in conjunction with a staircase procedure (2.41 down/1 up) tracked estimates of the contrast threshold corresponding to 75% correct. No feedback was provided regarding correct versus incorrect responses. Eight independent estimates were averaged to define the contrast threshold at each location. Contrast thresholds for Vernier targets with 18- and 36-min gaps were defined by averaging the thresholds for single filtered lines above and below fixation. Filtered Vernier targets were then presented at 2, 4, and 8 times their contrast thresholds (contrast threshold units, CTU). Vernier thresholds were determined by the method of constant stimuli. Within each block of 70 trials, the upper test line could be presented at one of seven positions: offset by 1, 2, or 3 units to the right or left of the lower reference line, or aligned with it. The order of presentation was randomized. The observer's task was to discriminate in which direction the upper test line was shifted with respect to the lower reference line. Unlike the contrast-detection task, auditory feedback was provided after each trial as to whether the observer's response was correct. We defined Vernier thresholds as the offset required to increase the probability of a "rightward" response from 50% to 84%. The results presented for each observer and condition represent the average of six–eight independent threshold estimates.

Data were collected for two well-trained, young-adult observers, who were unaware of the experimental hypothesis. Observer KN was emmetropic; TN wore a −0.50 D correction in front of her tested right eye. Each subject voluntarily granted written informed consent after the procedures of the experiment were explained and before the commencement of data collection.

3. RESULTS

Vernier thresholds for equally detectable, 3.3-c/deg targets are plotted as a function of target contrast in Fig. 2 for abutting and nonabutting targets with an interline gap of 18 or 36 arc min. Consistent with previous reports,[4,17,20–24] Vernier thresholds for abutting line targets improve approximately in proportion to the target contrast over the range we tested. On log–log axes (Fig. 2, left panel), the lines that best fit the data for the four velocities have slopes ranging between −0.68 and −0.94,

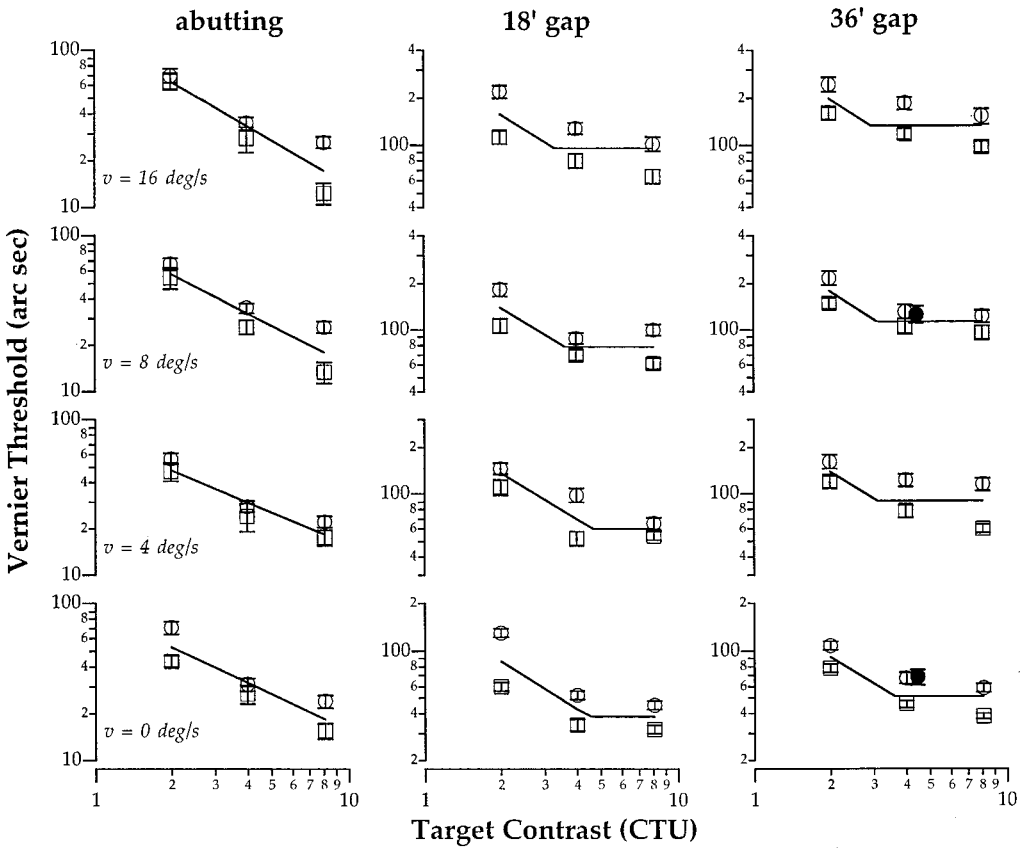

Fig. 2. Vernier thresholds (arc sec) are plotted as a function of target contrast (contrast threshold unit, CTU) for 3.3-c/deg targets, with target velocity as parameter. The target velocities are, from bottom to top, 0, 4, 8, and 16 deg/s. Targets were abutting lines (left) or lines that were separated by a gap of 18 (middle) or 36 arc min (right). Data were obtained from two observers (squares for KN and circles for TN). The single (for abutting targets) or double power functions (two-line fit, for separated targets) were fitted to the aggregate data of both observers. The two filled circles added to the plots for an interline gap of 36 arc min, at 0 and 8 deg/s, are data from a control experiment (see Section 4), in which horizontal lines were drawn on the monitor but were viewed as vertical lines through a Dove prism. Error bars represent ±1 standard error of the mean (s.e.m.).

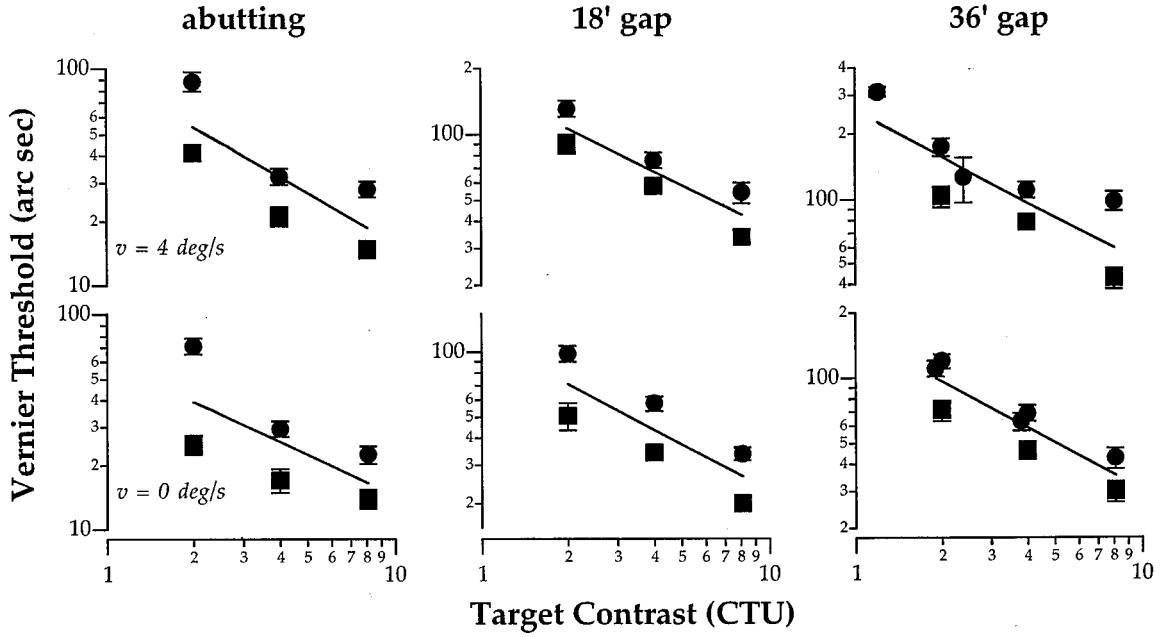

Fig. 3. Vernier thresholds (arc sec) are plotted as a function of target contrast (contrast threshold unit, CTU) for 6.6-c/deg targets that were either stationary (bottom), or moved at 4 deg/s (top). Details of the figure are as in Fig. 2, with the exception that each set of data was fitted with a single power function. For observer TN, some additional data were obtained for an interline separation of 36 arc min. Although plotted in the figure, these additional data were not used in any of the statistical analyses.

which do not differ significantly from one another (multiple regression analysis with dummy variables: t-value for slope ranges from -0.74 to $+0.28$, $p = 0.47$ to 0.78). Vernier thresholds for equally detectable stationary and moving abutting targets exhibit no systematic difference (repeated-measures analysis of variance (ANOVA): $F_{(df=3,3)} = 1.27, p = 0.46$). For example, at a contrast of 8× CTU, the average Vernier thresholds for the four velocities range between 16.9 and 17.6 arc sec.

Vernier thresholds for nonabutting targets show several differences from those for abutting targets. As expected, thresholds are higher for nonabutting than for abutting targets (repeated-measures ANOVA, $F_{(df=2,2)} = 314.7, p = 0.036$) and worsen with the interline separation (Fig. 2 middle and right panels). Also, consistent with the findings of Waugh and Levi[10] for broadband line targets, Vernier thresholds for the nonabutting targets improve over only a restricted range of contrast. Specifically, the Vernier thresholds for a target contrast of 2× CTU are significantly higher than those for target contrasts of 4× CTU ($F_{(df=1,1)} = 622.6, p = 0.022$) and 8× CTU ($F_{(df=1,1)} = 1021.9, p = 0.017$), but the Vernier thresholds for target contrasts of 4× CTU and 8× CTU do not differ reliably [$F_{(df=1,1)} = 49.1, p = 0.076$]. We therefore adopted a fitting strategy similar to that of Waugh and Levi[10] and assumed that Vernier thresholds improve initially in proportion to stimulus contrast (slope $= -1$ on log–log axes) and then saturate at some suprathreshold contrast value (slope $= 0$). For simplicity, we shall refer to the pair of lines with slopes of -1 and 0 as a two-line fit. The contrast at which the Vernier threshold saturates is indicated by the intersection of the two lines that best fit the aggregate data of the two observers. This analysis indicates that saturation occurs at an average of 3.60 (±0.65) times the contrast threshold for both stationary and moving nonabutting Vernier targets. The contrast level at which threshold saturation occurs is independent of both the image velocity (two-factor ANOVA: $F_{(df=3,3)} = 2.23, p = 0.264$) and the interline gap [$F_{(df=1,3)} = 8.28, p = 0.064$]. Finally, unlike the results for abutting Vernier targets, thresholds for nonabutting targets worsen systematically as a function of image velocity (repeated-measures ANOVA: $F_{(df=3,3)} = 176.0, p = 0.048$; see Fig. 2 and Fig. 4 below). For instance, Vernier thresholds for a target contrast of 8× CTU worsen by factors of 2.15 and 2.64 when the velocity of the targets increases from 0 (stationary) to 16 deg/s for interline gaps of 18 and 36 arc min, respectively.

Vernier thresholds for 6.6-c/deg targets are presented in Fig. 3. Consistent with the results obtained for 3.3-c/deg targets, Vernier thresholds are similar for equally detectable stationary and moving abutting 6.6-c/deg targets (repeated-measures ANOVA: $F_{(df=1,1)} = 24.27, p = 0.13$). Also, Vernier thresholds for nonabutting targets are affected similarly by target motion. In the presence of 4-deg/s target motion, Vernier thresholds for 6.6-c/deg targets with a contrast of 8×CTU are elevated by factors of 1.63 and 1.94 for 18- and 36-min gaps, respectively, compared with factors of 1.55 and 1.83 for 3.3-c/deg targets.

Differences also exist between the data for 3.3- and 6.6-c/deg targets. In general, Vernier thresholds are lower for 6.6- than for 3.3-c/deg targets, as expected from the approximately inverse relationship between Vernier thresholds and the spatial-frequency content of the target.[18,25–28] However, unlike in our previous study,[18] the Vernier thresholds for 6.6-c/deg targets are not half as low as those for 3.3-c/deg targets, an outcome that we attribute to a practice effect. Further, contrary to the results for 3.3-c/deg targets, Vernier thresholds for 6.6-c/deg nonabutting targets do not obviously saturate within the range of contrast tested. In particular, pairwise statistical comparisons indicate that only the Vernier thresholds for target contrasts of 2× CTU and 8× CTU differ significantly [$F_{(df=1,1)} = 209.4, p = 0.037$]. We therefore fitted each data set with a single power function (straight line on log–log axes). Across all conditions, these lines do not differ significantly from one another or from the average line (multiple regression with dummy variables: t-value for slope ranges from -0.43 to $+0.62$; $p = 0.54$ to 0.88). The slope for stationary abutting targets, -0.63 ± 0.26, is within the range of the slopes reported in previous studies when comparable stimuli were used. Specifically, when sine-wave stimuli were used, the exponent of the power function relating Vernier threshold to contrast decreased from -0.94 to -0.45 according to Whitaker,[27] and from -0.84 to -0.63 according to Levi *et al.*[28] as the grating spatial frequency increased from 1 to 8 c/deg. On the other hand, previous studies that used broadband line Vernier targets reported power functions with exponents close to -1.[4,17,20,22–24]

4. CONTROL EXPERIMENT

Because the stimuli in this study were presented on a raster display, we were concerned that the Vernier thresholds during target motion might have been contaminated by the time required to scan from the top to the bottom of the display. Specifically, the top line of the Vernier target is drawn slightly earlier than the bottom line, which, when the target is in motion, would be expected to introduce a slight horizontal offset. This offset should be larger for nonabutting than for abutting targets because the time required to scan between the two Vernier lines increases with their vertical separation. For instance, at 4-deg/s target motion, the spatial offset artifacts introduced by our display (assuming zero phosphor persistence) should be approximately 8, 16, and 23 arc sec for targets that are abutting and separated by 18 and 36 arc min, respectively. These artifacts are inadequate to account for the differences in thresholds for the three gap conditions (see Figs. 2 and 3). Nevertheless, to evaluate this potential artifact empirically, we retested observer TN, using targets that were drawn horizontally instead of vertically on the monitor, thereby virtually eliminating any time difference between presentation of the two Vernier lines. Targets were 3.3 c/deg, with an interline gap of 36 arc min and a velocity of either 0 or 8 deg/s, presented at 4× CTU. Viewing was through a Dove prism, oriented such that physically horizontal Vernier targets appeared vertical, as in the experiments described above. The observer reported the direction of offset between the "upper" and "lower" lines. As shown by the filled symbols in Fig. 2, Vernier thresholds obtained with horizontal

targets viewed through a Dove prism are remarkably similar to those obtained with the original vertical targets (open symbols), suggesting that raster delay had very little effect on our original results.

5. DISCUSSION

In this study we showed that unlike for abutting targets, Vernier thresholds for nonabutting, band-limited targets are affected by motion, even when target detectability is equated for. Previously we argued that the elevation of Vernier thresholds for abutting, broadband lines in motion occurs because the visual system shifts its sensitivity to progressively larger spatial filters.[17] By using band-limited targets, we sought to ensure that the visual system would use spatial filters tuned to essentially the same spatial frequency to analyze targets that moved at various velocities. Presumably, if the same set of spatial-frequency filters are provided with equally detectable targets, and if the outputs of these filters determine Vernier threshold, then Vernier thresholds should remain unchanged, regardless of velocity. Clearly, results like those shown in Fig. 2, left panel, for bandpass-filtered, abutting Vernier targets are consistent with these presumptions. The results presented in Fig. 2, middle and left panels, indicate that the mechanism that encodes the Vernier offset between two separated, bandpass-filtered lines is not similarly robust to target motion. The differential motion tolerance of abutting versus nonabutting Vernier targets is consistent with the widely held belief that the mechanisms underlying Vernier discrimination for the two types of target configurations are different. Presumably, Vernier thresholds for nonabutting targets are not mediated solely by the contrast responses of linear, oriented cortical filters that straddle the Vernier offset, as is thought to be the case for abutting targets.

According to Hering[13] (also see Weymouth *et al.*[29]), each retinal receptor stimulated by a Vernier line will signal a local sign. The visual system collects the local signs along the length of a line and assigns a mean local sign to this line. Position acuity is achieved by comparing the mean local signs assigned to the two lines of a Vernier target. Presumably, the precision of position acuity is enhanced because of the averaging process in which numerous samples are taken into account to derive the mean local sign. We now know that averaging along the length of a line is not crucial in achieving fine thresholds, because equivalent Vernier thresholds can be obtained from both line and dot stimuli.[7,30] In fact, thresholds in the hyperacuity range can be achieved even if the separated targets are composed of clusters of dots[31–33] or irregular shapes[34] or have opposite contrast polarity.[11,35–38] These findings are in consonance with the notion that as long as a mean local sign can be computed for each element of a Vernier target, regardless of the target configuration, then the visual system can compare the two local signs and derive a relative-position signal between the two elements. To date, it is still unclear how the second-stage comparison process is carried out; however, recent evidence from masking experiments[39] and from experiments that used Vernier targets composed of opposite-polarity elements[12] suggest that large, nonlinear rectifying collator filters may be involved.

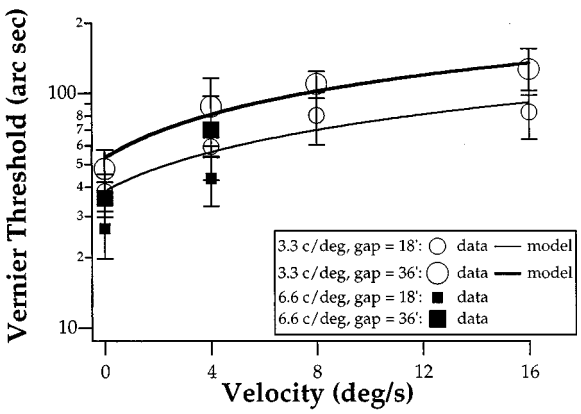

Fig. 4. Vernier threshold (±1 s.e.m.) for targets presented at 8× CTU is plotted as a function of target velocity, for 3.3- and 6.6-c/deg nonabutting targets. The solid curves represent the predictions of an additive-variance model fit to the results for 3.3-c/deg targets with a contrast of 8× CTU. Similar fits were applied to the Vernier thresholds obtained for targets of lower contrast (see text and Table 1 for details).

Implicit in the discussion above, and explicit in the collator model proposed by Levi and colleagues,[12,39] is that the comparison between mean local signs should be independent of the characteristics of the Vernier stimulus, including its spatial-frequency content.[36] We would therefore expect that the motion-induced threshold elevation for nonabutting Vernier targets should be similar for 3.3- and 6.6-c/deg targets. Figure 4 plots the Vernier thresholds for 3.3-c/deg targets with a contrast of 8× CTU as a function of target velocity for each interline gap. The solid curves in Fig. 4 depict the predictions of an additive-variance model (see below). For comparison, we also show the average Vernier thresholds for 6.6-c/deg targets at eight times the contrast-detection threshold. At 4 deg/s (the only velocity at which we can compare the data for 3.3- and 6.6-c/deg targets), it is clear that the motion-induced threshold elevations are virtually identical, consistent with the operation of a local-sign mechanism for nonabutting Vernier targets.

A. Additive-Variance Model

Why is the local-sign mechanism susceptible to degradation by target motion, whereas the spatial-filter mechanism is not? For moving targets, a critical distinction may be that information about Vernier offset becomes available to the local-sign mechanism only after two distinct (sets of) receptive fields are compared, whereas information about offset is obtained initially within the individual receptive fields of a spatial-filter mechanism. Consequently, for the local-sign mechanism to encode the offset of a moving Vernier stimulus accurately, the separate cortical map locations of each target element must be compared simultaneously. Random temporal fluctuations with respect to precise synchrony would be expected to introduce noise in this comparison process by producing spurious signals of spatial offset that increase with the amount of temporal asynchrony and the stimulus velocity. This source of position noise is a central feature of

the additive-variance model that we present here to account for the velocity-dependent elevation of Vernier thresholds for nonabutting targets.

Three factors are assumed to contribute to the elevation of Vernier threshold for moving, nonabutting targets. First, a minimum variance (Th_0) that varies inversely with the contrast of the Vernier target is assumed to exist in determining the map locations for each of the Vernier lines. Because our targets were equated at each velocity for detectability, the variance for determining the locations of the Vernier lines should be independent of velocity and therefore can be estimated from the stationary Vernier threshold. Additional variance is assumed to accrue as the gap between the Vernier targets, G, increases, in accordance with the well-established proportional relationship between the stationary Vernier threshold and interelement separation.[7–9,30,40] Second, as explained above, random temporal asynchronies in comparing the map locations of the two separate Vernier elements should result in spurious signals of offset, which increase with the stimulus velocity, V. Third, to account for the greater influence of velocity on thresholds for more widely separated Vernier targets (see Section 3), we assume that the range of these temporal asynchronies increases with separation of the stimuli, as represented on the cortical map. Another, fourth, factor is assumed to partly mitigate the deleterious effect of target velocity on Vernier threshold. Specifically, although random temporal asynchronies in the comparison process should increase the offset variance for a Vernier target in motion, this variance should decrease according to the number of local-sign comparisons that are made. To a first approximation, we assume that the number of map locations compared is proportional to the spatial extent of target motion and therefore increases linearly with velocity.

Our model assumes that the Vernier threshold for nonabutting targets is given by the square root of the summed sources of variance as listed above:

$$\text{gap Vernier threshold} = \sqrt{(Th_0)^2 + (k_3G)^2 + \frac{[(k_1V)^2 + (k_2GV)^2]}{k_4V}}, \quad (1)$$

where

Th_0 = optimal threshold, in degrees, for a stationary Vernier target with 0.3-deg (18-arc-min) gap;

G = gap, in deg, specified as (actual gap size − 0.3 deg);

V = target velocity, in degrees per second;

k_3G = elevation in optimal threshold associated with increasing Vernier gap;

k_1V = effect on threshold of temporal asynchronies in the comparison process;

k_2GV = effect on threshold of additional comparison noise associated with increasing target gap;

k_4V = number of separate local-sign comparisons for a target in motion.

To determine whether our data for nonabutting Vernier stimuli are consistent with the above model, we used the average thresholds for a 3.3-c/deg stationary Vernier target with a separation of 18 arc min (Fig. 2, middle bottom panel) as estimates of Th_0. Separate values of Th_0 were used for each contrast of the Vernier target (Table 1). The constants k_1–k_4 were then obtained with the SAS (Cary, N.C.) NLIN nonlinear regression procedure with an iterative search method and a least-squares criterion. For each contrast value the model was fitted simultaneously to the optimal thresholds for 3.3-c/deg Vernier targets with 18- and 36-arc-min gaps (Fig. 2, middle and right panels). Overall, the model provides excellent fits to the 3.3-c/deg data for all three contrasts of the Vernier target (2× CTU: $r^2 = 0.997$, $F_{(df=3,5)} = 481.0$, $p < 0.001$; 4× CTU: $r^2 = 0.997$, $F_{(df=3,5)} = 588.9$, $p < 0.001$; 8× CTU: $r^2 = 0.993$, $F_{(df=3,5)} = 245.6$, $p < 0.001$). As an example, the model fits to Vernier thresholds for targets that are eight-times the contrast threshold are depicted by the solid curves in Fig. 4.

The best-fitting model parameters for all three target contrasts are given in Table 1. In the rightmost expression under the square root sign in Eq. (1), note that the target velocity, V, appears in both terms of the numerator and in the denominator. Consequently, V was removed from the denominator of this expression by division before the model was evaluated to prevent the denominator from vanishing when V is equal to zero. Further consideration of the rightmost expression under the square root sign indicates that k_1, k_2, and k_4 are not independent parameters and could be replaced by just two fitted constants: $k_1/\sqrt{k_4}$ and $k_2/\sqrt{k_4}$. For heuristic reasons, we prefer the form of the model that is given by Eq. (1) and presume that independent estimates for k_1, k_2, and k_4 would be obtainable if additional experiments were conducted. To fit the model to our data, we fixed the value of k_4 at 1. Implicitly, this assumes that the same number of local-sign comparisons are made for a stationary 3.3-c/deg Vernier target and one that moves at 1 deg/s (i.e., a distance of 0.15°) for 150 ms.

Table 1. Best-Fit Parameters (±1 s.e.m.) for Additive-Variance Model

Parameter (units)	2× CTU	4× CTU	8× CTU
Th_0 (deg)	0.0261	0.0118	0.0107
k_1 (s)	0.0100 ± 0.000739	0.00671 ± 0.000389	0.00572 ± 0.000528
k_2 (s/deg)	0.0279 ± 0.00545	0.0240 ± 0.00247	0.0210 ± 0.00329
k_3 (unitless)	0.0279 ± 0.0294	0.0395 ± 0.00765	0.0338 ± 0.0106
k_4 (s/deg)	1	1	1

B. Contrast Dependence

Previously, Vernier thresholds for nonabutting, stationary broadband targets were reported to improve with contrast only up to approximately three times the contrast-detection threshold.[10,41] Our data for 3.3-c/deg targets are consistent with this result and extend it to nonabutting Vernier targets in motion. In particular, Vernier thresholds for nonabutting targets appear to saturate at a contrast that is between 3 and 4× CTU (Fig. 2). However, data for 6.6-c/deg nonabutting targets show greater contrast dependence. Although the Vernier thresholds for these 6.6-c/deg targets do not clearly saturate within the range of contrast levels that we tested, a conservative estimate of the contrast at which threshold saturation occurs can be found by applying two-line fits to the aggregate data of the two observers. Across the nonabutting conditions for the 6.6-c/deg Vernier targets, these estimates average 5.67 ± 0.52 times the contrast threshold, which is significantly higher than that for 3.3-c/deg targets (t-test: $t_{(df=10)} = 5.50$, $p < 0.0003$).

What could account for the different contrast dependence for 3.3- versus 6.6-c/deg nonabutting targets? Numerous neurophysiological studies have shown that neuronal activities in response to contrast differ for low- versus high-spatial-frequency stimuli.[42–44] Specifically, for low-spatial-frequency stimuli, the neuronal responses increase rapidly with stimulus contrast and tend to saturate at moderate contrast levels. In comparison, for high-spatial-frequency stimuli, the neuronal responses increase at a slower rate with stimulus contrast and saturate at a higher level of stimulus contrast.[42,43] On the basis of their data, Sclar *et al.*[44] suggested that the contrast level at which response saturation occurs approximates an inversely proportional relationship to the square root of the stimulus area. These findings are qualitatively consistent with the greater contrast dependence of 6.6- than 3.3-c/deg Vernier stimuli.

ACKNOWLEDGMENTS

We thank Ying-sheng Hu for statistical assistance. The HIPS software was made available by the courtesy of Gordon Legge and the Minnesota Laboratory for Low-Vision Research. This research was supported by research grant R01-EY05068 (to H. E. Bedell) and core grant P30-EY07551 from the National Eye Institute and by an Ezell Fellowship from the American Optometric Foundation (to S. T. L. Chung).

*Address correspondence to Harold E. Bedell: e-mail, HBedell@mail-gw.opt.uh.edu.

REFERENCES

1. G. Westheimer, "Visual acuity and hyperacuity," Invest. Ophthalmol. **14**, 570–572 (1975).
2. G. Westheimer, "The spatial sense of the eye," Invest. Ophthalmol. Visual Sci. **18**, 893–912 (1979).
3. J. M. Findlay, "Feature detectors and Vernier acuity," Nature (London) **241**, 135–137 (1973).
4. H. R. Wilson, "Responses of spatial mechanisms can explain hyperacuity," Vision Res. **26**, 453–469 (1986).
5. S. J. Waugh, D. M. Levi, and T. Carney, "Orientation, masking, and Vernier acuity for line targets," Vision Res. **33**, 1619–1638 (1993).
6. T. Carney and S. A. Klein, "Optimal spatial localization is limited by contrast sensitivity," Vision Res. **39**, 503–511 (1999).
7. G. D. Sullivan, K. Oatley, and N. S. Sutherland, "Vernier acuity as affected by target length and separation," Percept. Psychophys. **12**, 438–444 (1972).
8. S. A. Klein and D. M. Levi, "Position sense of the peripheral retina," J. Opt. Soc. Am. A **4**, 1543–1553 (1987).
9. D. M. Levi and S. A. Klein, "The role of separation and eccentricity in encoding position," Vision Res. **30**, 557–585 (1990).
10. S. J. Waugh and D. M. Levi, "Visibility and Vernier acuity for separated targets," Vision Res. **33**, 539–552 (1993).
11. R. P. O'Shea and D. E. Mitchell, "Vernier acuity with opposite-contrast stimuli," Perception **19**, 207–221 (1990).
12. D. M. Levi and S. J. Waugh, "Position acuity with opposite-contrast polarity features: evidence for a nonlinear collector mechanism for position acuity?" Vision Res. **36**, 573–588 (1996).
13. E. Hering, "Über die Grenzen der Sehscharfe," Ber. Math. Phys. Classe konig. sachs. Ges. Wiss. (Leipzig) 16–24 (1899); cited by Levi and Waugh (Ref. 12).
14. G. Westheimer and S. P. McKee, "Visual acuity in the presence of retinal image motion," J. Opt. Soc. Am. **65**, 847–850 (1975).
15. M. J. Morgan and S. Benton, "Motion-deblurring in human vision," Nature **340**, 385–386 (1989).
16. T. Carney, D. A. Silverstein, and S. A. Klein, "Vernier acuity during image rotation and translation: visual performance limits," Vision Res. **35**, 1951–1964 (1995).
17. S. T. L. Chung, D. M. Levi, and H. E. Bedell, "Vernier in motion: What accounts for the threshold elevation?" Vision Res. **36**, 2395–2410 (1996).
18. S. T. L. Chung and H. E. Bedell, "Moving Vernier with band-pass filtered stimuli," Invest. Ophthalmol. Visual Sci. (Suppl.) **37**, S734 (1996).
19. M. S. Landy, Y. Cohen, and G. Sperling, "HIPS: image processing under UNIX. Software and applications," Behav. Res. Methods Instrum. Comput. **16**, 199–216 (1984).
20. S. A. Klein, E. Casson, and T. Carney, "Vernier acuity as line and dipole detection," Vision Res. **30**, 1703–1719 (1990).
21. M. J. Morgan and T. S. Aiba, "Vernier acuity predicted from changes in the light distribution of the retinal image," Spatial Vis. **1**, 151–161 (1985).
22. T. Banton and D. M. Levi, "Binocular summation in Vernier acuity," J. Opt. Soc. Am. A **8**, 673–679 (1991).
23. S. J. Waugh and D. M. Levi, "Visibility, timing, and Vernier acuity," Vision Res. **33**, 505–526 (1993).
24. J. Krauskopf and B. Farell, "Vernier acuity: effects of chromatic content, blur and contrast," Vision Res. **31**, 735–749 (1991).
25. A. Bradley and B. C. Skottun, "Effects of contrast and spatial frequency on Vernier acuity," Vision Res. **27**, 1817–1824 (1987).
26. D. Whitaker and D. MacVeigh, "Interation of spatial frequency and separation in Vernier acuity," Vision Res. **31**, 1205–1212 (1991).
27. D. Whitaker, "What part of a Vernier stimulus determines performance?" Vision Res. **33**, 27–32 (1993).
28. D. M. Levi, S. A. Klein, and H. Wang, "Discrimination of position and contrast in amblyopic and peripheral vision," Vision Res. **34**, 3293–3313 (1994).
29. F. W. Weymouth, E. E. Andersen, and H. L. Averill, "Retinal mean local sign: a new view of the relation of the retinal mosaic to visual perception," Am. J. Physiol. **63**, 410–411 (1923).
30. G. Westheimer and S. P. McKee, "Spatial configurations for visual hyperacuity," Vision Res. **17**, 941–947 (1977).
31. D. Whitaker and H. Walker, "Centroid evaluation in the Vernier alignment of random dot clusters," Vision Res. **28**, 777–784 (1988).
32. R. F. Hess, S. R. Dakin, and D. Badcock, "Localization of el-

ement clusters by the human visual system," Vision Res. **34**, 2439–2451 (1994).
33. D. R. Badcock, R. F. Hess, and K. Dobbins, "Localization of element clusters: multiple cues," Vision Res. **36**, 1467–1472 (1996).
34. S. S. Patel, H. E. Bedell, and M. T. Ukwade, "Vernier judgments in the absence of regular shape information," Vision Res. **39**, 2349–2360 (1999).
35. D. M. Levi and G. Westheimer, "Spatial interval discrimination in the human fovea: What delimits the interval?" J. Opt. Soc. Am. A **4**, 1304–1313 (1987).
36. C. A. Burbeck, "Position and spatial frequency in large-scale localization judgments," Vision Res. **27**, 417–427 (1987).
37. A. Toet, "Visual perception of spatial order," Ph.D. dissertation (Ryksuniversiteit, Utrecht, The Netherlands, 1987).
38. D. M. Levi, B. Jiang, and S. A. Klein, "Spatial interval discrimination with blurred lines: Black and white are separate but not equal at multiple spatial scales," Vision Res. **30**, 1735–1750 (1990).
39. A. J. Mussap and D. M. Levi, "Spatial properties of filters underlying Vernier acuity revealed by masking: evidence for collator mechanisms," Vision Res. **36**, 2459–2473 (1996).
40. A. Toet, H. L. van Eekhout, J. J. Simons, and J. J. Koenderink, "Scale invariant features of differential spatial displacement discrimination," Vision Res. **27**, 441–452 (1987).
41. R. F. Hess and I. E. Holliday, "The coding of spatial position by the human visual system: effects of spatial scale and contrast," Vision Res. **32**, 1085–1097 (1992).
42. E. Kaplan and R. M. Shapley, "The primate retina contains two types of ganglion cells, with high and low contrast sensitivity," Proc. Natl. Acad. Sci. USA **83**, 2755–2757 (1986).
43. D. H. Hubel and M. S. Livingstone, "Color and contrast sensitivity in lateral geniculate body and primary visual cortex of the macaque monkey," J. Neurosci. **10**, 2223–2237 (1990).
44. G. Sclar, J. H. R. Maunsell, and P. Lennie, "Coding of image contrast in central visual pathways of the macaque monkey," Vision Res. **30**, 1–10 (1990).